C. R. Physique 3 (2002) 667–676

Solides, fluides : propriétés électroniques et optiques/*Solids, fluids: electronic and optical properties*

L'EFFET HALL QUANTIQUE FRACTIONNAIRE
THE FRACTIONAL QUANTUM HALL EFFECT

Probing spin physics in the quantum Hall regime by heat capacity and magnetotransport measurements

Sorin Melinte [a,b]*, Mansour Shayegan [a], Vincent Bayot [b]

[a] **Department of Electrical Engineering, Princeton University, Princeton, NJ 08544, USA**

[b] **Research Center on Microscopic and Nanoscopic Electronic Devices and Materials (CERMIN), Université Catholique de Louvain, B-1348 Louvain-la-Neuve, Belgium**

Received 7 March 2002; accepted 15 May 2002

Note presented by Guy Laval.

Abstract We review recent heat capacity and magnetotransport experiments on GaAs/AlGaAs heterostructures containing multilayer two-dimensional electron systems (2DESs) in the quantum Hall regime. Emphasis in this article is on the study of the heat capacity near Landau level filling factor $\nu = 1$. We also present a detailed survey of the development of the quantum Hall effect in tilted-magnetic fields for $\nu \lesssim 2$. Among the novel phenomena we address is the strong coupling between the nuclear spins and the electrons associated with the spin phase transitions of the 2DES at $\nu = 4/3$ and near $\nu = 1$. ***To cite this article: S. Melinte et al., C. R. Physique 3 (2002) 667–676.***

quantum Hall effect / two-dimensional electron systems / spin dynamics / phase transitions / heat capacity / magnetotransport

Physique de spin dans l'effet Hall quantique par des expériences de chaleur spécifique et de magnétotransport

Résumé Nous présentons une revue des expériences de chaleur spécifique et de magnétotransport effectuées récemment sur des hétérostructures constituées d'une multicouche de système bidimensionnel d'électrons dans le régime d'effet Hall quantique. L'article met l'accent sur les études de chaleur spécifique au voisinage du facteur de remplissage des niveaux de Landau $\nu = 1$. Nous présentons aussi une revue détaillée du développement de l'effet Hall quantique en champ magnétique incliné pour $\nu \lesssim 2$. Parmi les nouveaux effets observés, nous discutons le fort couplage entre spins nucléaires et les électrons associé aux transitions de phase du système électronique à $\nu = 4/3$ et au voisinage de $\nu = 1$. ***Pour citer cet article : S. Melinte et al., C. R. Physique 3 (2002) 667–676.***

effet Hall quantique / système bidimensionnels d'électrons / dynamique de spin / transition de phase / chaleur spécifique / magnétotransport

* Correspondence and reprints.
E-mail address: sorin@pcpm.ucl.ac.be (S. Melinte).

S1631-0705(02)01355-5/FLA

1. Introduction

The quantum Hall effect (QHE), observed in two-dimensional electron systems (2DESs) in high magnetic fields and low temperatures, comprises two united aspects – one originating from the quantization of the electronic motion into Landau levels [1], the other stemming from electron–electron interactions [2]. The significance of the electronic spin degree of freedom and the possibility of ferromagnetic ordering in the QHE regime was anticipated early on [3]. Started by a series of influencial works on the QHE state at Landau level filling factor $\nu = 1$ [4,5], QHE ferromagnetism is one of the most interesting, recently appeared developments. At $\nu = 1$ the 2DES is an itinerant ferromagnet with a quantized Hall coefficient and its low energy spin excitations are *skyrmions* – spin textures accommodating precisely one unit of charge. The presence of skyrmions in the $\nu = 1$ QHE ground state results in novel properties that have been recently probed by magnetotransport [6], optically pumped nuclear magnetic resonance [7–9], heat capacity [10–12], and other spectroscopic means [13–15]. One of the peculiarities of the $\nu = 1$ QHE ferromagnet is the skyrmion-induced, large nuclear spin–lattice relaxation rate which manifests as a giant contribution of the nuclear spins to the measured heat capacity. It is the purpose of this paper to review recent heat capacity experiments near $\nu = 1$. In particular, our motivation is to address the problem of how strong Zeeman energy affects the stability of skyrmions.

Pre-skyrmion era experiments [16,17] investigated rather thoroughly the spin configurations of various fractional QHE states (e.g., $\nu = 2/3$) and provided us with a basic understanding of spin phase transitions in the 2DES in terms of charge excitations carrying a spin. Recently, measurements of Kronmüller et al. [18] revealed new, unexpected resistance maxima near $\nu = 2/3$ and suggested that QHE ground states might also be influenced by the nuclear polarization of nuclei inside the GaAs quantum wells (QWs). A number of subsequent experiments [19,20] have provided further evidence connecting the anomalous magnetotransport around $\nu = 2/3$ with the hyperfine interaction [21] between the nuclear spins and the two-dimensional (2D) electrons. However, mainly because magnetoresistance was measured, several concerns are still matter of debate. One interesting question is whether nuclear spins are also involved in the physics of the $\nu = 4/3$ QHE state, which is equally a well-documented example [22,23] for spin phase transitions in the fractional QHE regime. In this respect, a unique opportunity to study the role of nuclear spins in the QHE regime is offered by heat capacity studies [10,12]. We present here magnetotransport and heat capacity measurements near $\nu = 4/3$ as the Zeeman energy is increased by adding a component of the magnetic field parallel to the 2DES. We find a spin phase transition at $\nu = 4/3$ in our investigated samples and compare the evolution of the $\nu = 4/3$ QHE state in tilted-magnetic fields with heat capacity results [12]. These data provide additional pieces of evidence for nuclear spin related phenomena in the fractional QHE regime.

The plan of the paper is as follows. Section 2 is devoted to experimental details. Included is a description of the samples, followed by brief accounts of magnetotransport and heat capacity techniques employed here. Section 3 contains our main results. In Section 4.1 we concentrate on heat capacity data at filling factors close to unity. The interrelation between the re-entrant behavior of the $\nu = 4/3$ QHE state and nuclear spins is discussed in Section 4.2. In section 5 we summarize our findings and we conclude the paper with remarks about possible future directions.

2. Experimental methods

2.1. Samples

The data reported here were obtained on multiple-QW heterostructures grown by molecular beam epitaxy on $\langle 1\,0\,0\rangle$-oriented GaAs substrates. Details of the MBE system, wafer preparation, structure design, and growth procedure were given previously [24]. Two heterostructures (M242 and M280), each composed of one hundred GaAs QWs, were used in this study. The GaAs QWs are separated by AlGaAs barriers which are δ-doped with donors (Si) near their centers [24]; we used asymmetric δ-doping to compensate for the

migration of Si along the growth direction [25]. Sample M242 (M280) has 250 Å (300 Å) wide QWs, 1850 Å (2500 Å) thick $Al_{0.3}Ga_{0.7}As$ ($Al_{0.1}Ga_{0.9}As$) barriers, and nominal density $n = 1.4 \cdot 10^{11}$ cm^{-2} ($8.5 \cdot 10^{10}$ cm^{-2}).

2.2. Magnetotransport

All transport measurements were performed in a dilution refrigerator and the samples were positioned in situ at an angle θ between the direction of the magnetic field B and the normal to the plane of 2D electrons. We used 2×2 mm^2 samples with electrical contacts positioned in a van der Pauw geometry. The longitudinal (R_L) and Hall (R_H) resistances were measured using standard lock-in detection techniques. The value of the QHE excitation gap is determined from the temperature (T) dependence of R_L at the QHE minima. These dependencies are measured over a temperature range from 0.04 to 2 K. The framework which is useful in analyzing and interpreting the QHE excitation data has been excellently summarized by Boebinger et al. [26]. As in [26], we extract the excitation gap Δ_ν (expressed in K) at filling factor ν by fitting the expression $R_L(T) \propto \exp(-\Delta_\nu/2T)$ to the measured $R_L(T)$ data.

2.3. Heat capacity

For the purpose of heat capacity C measurements, samples were prepared by etching and polishing the material. The thinning of the excess bulk GaAs substrate was necessary to remove the indium present on the back of the samples from their molecular-beam–epitaxy block mount, and to improve the 2DES signal-to-background ratio [10]. For heat capacity experiments on M242 heterostructure we used a 7×7 mm^2 piece of the wafer thinned down to ≈ 65 μm. Specific-heat measurements on M280 heterostructure were carried on a 7×10 mm^2 piece of the wafer which was thinned down to ≈ 160 μm. Unfortunately, the expedient of using large area samples makes the density not entirely homogenous within a 2D electron layer. Typical density inhomogeneities across our measured specimens are ±3%. The transverse variation of density (from layer to layer) is ±2%. For C measurements, the M280 sample was tilted in situ at an angle $0° \lesssim \theta \lesssim 77°$. For M242 sample, the experimental arrangement did not include the rotating platform: C was measured while B was applied either perpendicular to the 2DES plane ($\theta = 0°$) or at a fixed angle of $\theta = 30 \pm 2°$.

In general, heat capacity is a bulk property with contribution from *all* components of a given thermodynamic system. In a multiple-QW heterostructure, at very low temperature, various types of heat capacities are encountered, each having its own T-dependence [10]. When the sample is placed in a magnetic field, besides lattice and electronic heat capacities, there might be an excess heat capacity due to nuclear spins. In our samples, in the high-T limit ($\Delta_n \ll k_B T$), the Schottky nuclear heat capacity of Ga and As atoms in the QWs is estimated at

$$C_n^{QW} = \begin{cases} 1.9 \cdot 10^{-11} B^2 T^{-2} \text{ (J/K)} & \text{for M242,} \\ 3.3 \cdot 10^{-11} B^2 T^{-2} \text{ (J/K)} & \text{for M280.} \end{cases}$$

Here T is expressed in K, B is given in T, $\Delta_n = \alpha_n B$ is the nuclear level spacing, and $\alpha_n/k_B = 4.9 \cdot 10^{-4}$, $6.23 \cdot 10^{-4}$ and $3.5 \cdot 10^{-4}$ (K/T) for ^{69}Ga (60.4%), ^{71}Ga (39.6%), and ^{75}As (100%), respectively [10].

3. Results

3.1. Magnetotransport data

Figure 1 shows R_L (left axis) and R_H (right axis) versus B at $T = 50$ mK and $\theta = 0°$ in sample M280. The high quality of the investigated multiple-QW samples is shown by the presence of strong fractional QHE states at $\nu = 2/5$ and $3/5$. Figure 2 illustrates magnetoresistance traces taken at $T = 50$ mK and various tilt angles in sample M280. A rather complex structure of the fractional QHE for $\nu \lesssim 2$ has been observed in

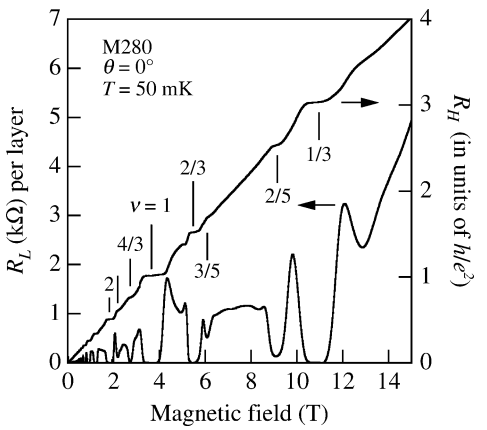

Figure 1. R_{L} (left axis) and R_{H} (right axis) versus B at $T = 50$ mK and $\theta = 0°$ (sample M280). The vertical lines indicate some prominent filling factors.

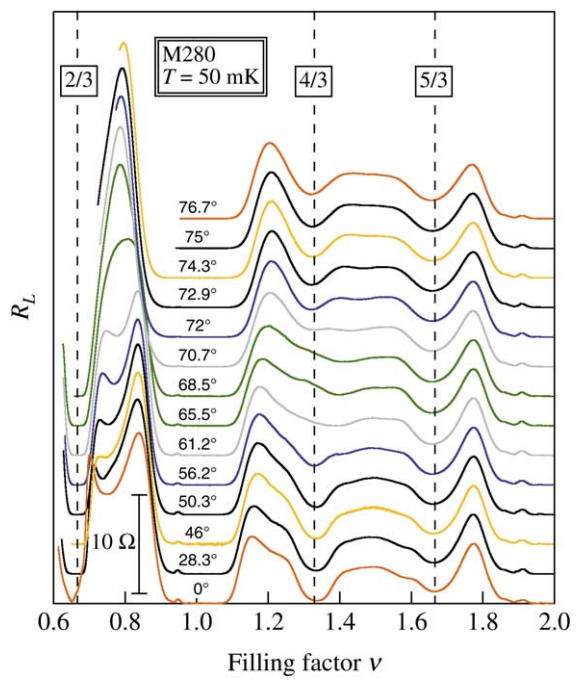

Figure 2. R_{L} versus ν at $T = 50$ mK and indicated tilt angles (sample M280). Curves are offset for clarity. The vertical dashed lines correspond to filling factors $\nu = 5/3$, $4/3$, and $2/3$.

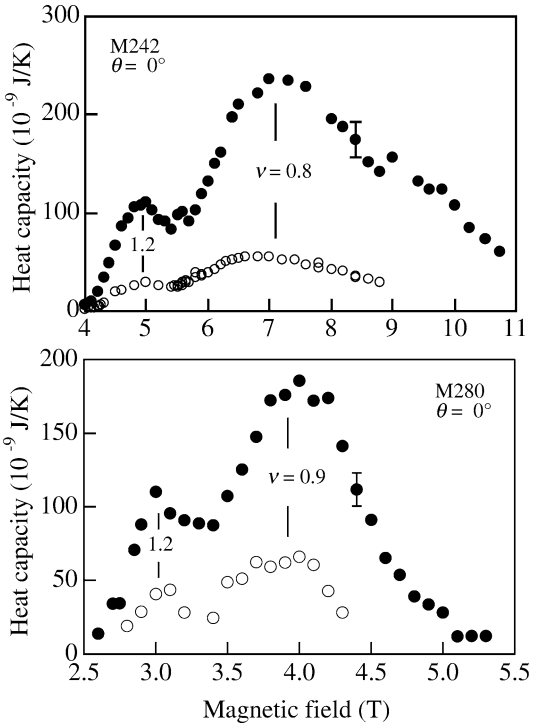

Figure 3. C versus B at $\theta = 0°$ for $T = 60$ mK (•) and $T = 100$ mK (○). Top (bottom) panel displays data taken on sample M242 (M280).

previous tilted magnetic field studies on single heterojunctions [22]. In the present data, several fractional QHE states are readily detectable: $\nu = 2/3$, $4/3$, and $5/3$. Only very small changes occurred around $\nu = 5/3$ by tilting the sample. The R_{L} minima at $\nu = 2/3$ and $\nu = 1$ became deeper in the case of tilted samples. On the other hand, at $\nu = 4/3$, the state weakens with increasing θ and it is absent for $\theta \gtrsim 65°$. We found, in fact, a *re-entrant* behavior for the $\nu = 4/3$ QHE state, as it re-emerges for $\theta \gtrsim 71°$ [22].

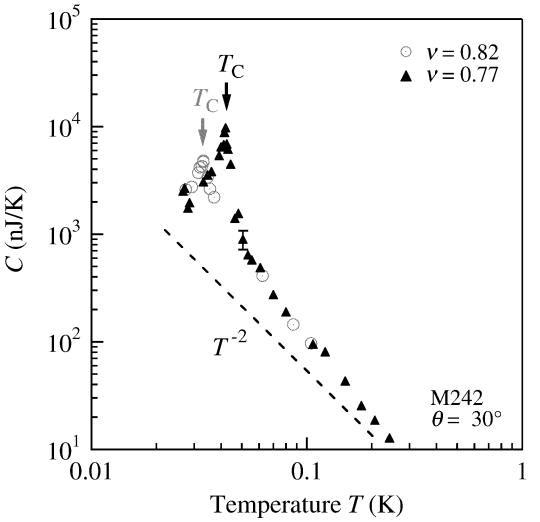

Figure 4. C versus T at $\theta = 30°$ and indicated values of ν (sample M242). The T^{-2} dependence expected for the Schottky effect is shown as a dashed line. T_c is marked by the vertical arrows.

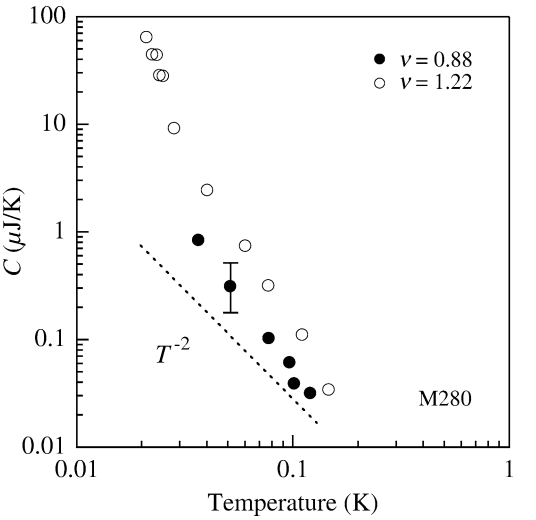

Figure 5. C versus T at $\theta = 0°$ ($\nu = 0.88$, filled circles) and $\theta = 71°$ ($\nu = 1.22$, open circles) is shown in a log–log plot (sample M280). The dashed line shows the T^{-2} dependence expected for the Schottky model.

3.2. Heat capacity data

Figure 3 shows C versus B at $\theta = 0°$ for $T = 60$ and 100 mK. Relative to its low-B magnitude (~ 10 pJ/K), which is consistent with C being dominated by the crystalline lattice and 2DESs contributions, C exhibits up to $\sim 10^5$-fold enhancement near $\nu = 1$. As shown in Fig. 3, the $\theta = 0°$ data are qualitatively similar for both investigated samples. A key point in Fig. 3 is that C exhibits broad maxima at $\nu \approx 0.8$ and $\nu \approx 1.2$, and decreases rapidly for $\nu \gtrsim 4/3$ and $\nu \lesssim 2/3$. The fact that C maxima appear nearly at the same ν in both samples is a *prima facie* evidence of the 2DES playing an important role for the anomalous C behavior. Figure 3 also captures the evolution of C versus B with temperature in samples M242 and M280: remarkably, in the vicinity of $\nu = 1$, C *increases* with decreasing T.

Figure 4 shows the T-dependence of C at $\theta = 30°$ for $\nu = 0.82$ and $\nu = 0.77$ in sample M242. The T^{-2} dependence expected for the nuclear Schottky effect is shown as a dashed line. We observe that the $C \propto T^{-2}$ behavior is followed only down to ≈ 60 mK. For $T \lesssim 60$ mK, C increases faster with decreasing T, and exhibits a remarkably sharp peak at T_c before decreasing at very low T. Figure 5 displays C versus T at $\theta = 0°$ ($\nu = 0.88$) and $\theta = 71°$ ($\nu = 1.22$) for sample M280 in a log–log plot. The dashed line shows the T^{-2} dependence expected for the Schottky model. The sharp peak in C versus T is not observed in sample M280, which might signal that it occurs at lower temperatures in this lower density heterostructure. The Schottky T-dependence is followed down to $T \approx 30$ mK. Interestingly, a marked non-Schottky behavior of the heat capacity is found at very low temperature at $\theta = 71°$ and $\nu = 1.22$, which is reminiscent of the sharp peak in C versus T observed in sample M242.

4. Discussion

4.1. Skyrmions

We begin with a discussion of Figs. 3–5 data in the T range where $C \propto T^{-2}$. Both the very large magnitude of C and the T^{-2} dependence point to the nuclear Schottky effect which results from the entropy reduction of the nuclear spin system with decreasing T when $\Delta_n \ll k_B T$. The observation of the Schottky effect requires good coupling of the nuclei to the lattice in order to reach thermal equilibrium

in the time scale of the experiment. This coupling is provided by electron spin–flip excitations and further relaxation to the lattice [21]. Consequently, while the effect is commonly observed in metals, it usually remains undetected in high purity materials with low free-carrier density. At first sight, because of their high purity and the low free-carrier density in the quantum wells, GaAs/AlGaAs heterostructures should not be good candidates for the observation of a nuclear Schottky effect. While this is supported by the low-B data [10] (not shown here) where only the lattice, addenda and 2DESs contribute to the low value of C, surprisingly a Schottky behavior is observed at higher B near $\nu = 1$. Based on previous experimental and theoretical work [4,5,7,8], we suggest that near $\nu = 1$ skyrmions induce a strong coupling of the nuclear spin system to the lattice and the large nuclear heat capacity is observed. The key role of skyrmions is supported by: (1) the absence of the nuclear-spin contribution to our measured C for $\nu \gtrsim 4/3$ and $\nu \lesssim 2/3$ where the skyrmions are no longer the ground state of the 2DES, and (2) our experiments in a tilted B (see below Figs. 6 and 7) which clearly show that the heat capacity anomaly relates to the 2DES filling factor (rather than total B).

The low-T peak in heat capacity has been attributed to a skyrmion solid-to-liquid phase transition [5]. We have performed quasi-adiabatic thermal experiments [11] revealing that the mechanism responsible for the peak in C versus T is a dramatic enhancement of nuclear spin diffusion across the QW–barrier interface. While only the nuclear heat capacity of the QWs' atoms is observed away from T_c, an increasing number of nuclei in the barriers contribute to the measured heat capacity when $T \to T_c$. The details of the skyrmion solid-to-liquid phase transition are largely unknown. We speculate that the C versus T peak is induced by the critical slowing down of the spin fluctuations in the 2DES, associated with the skyrmion liquid-to-solid phase transition. The critical slowing down causes the electron motion time scale to pass through the nuclear time scale. Hence, the QWs and barriers spectrally overlap (in the frequency domain) and the spin-diffusion across the QW–barrier interface is allowed *only* near T_c.

A useful, dimensionless parameter in describing heat capacity data is the ratio ξ of the measured C to C_n^{QW}. This ratio provides a measure of the QWs' nuclei which strongly couple to the lattice, and hence signals the presence of low-energy spin excitations in the 2DES associated to skyrmions. This manœuvre allows us to replace C versus B graphs (Fig. 3), by ξ versus ν plots (Fig. 6). Presented this way, the $\theta = 0°$ heat capacity data are highly symmetric around $\nu = 1$. We see in Fig. 6 that ξ shows maxima of the order of unity at $\nu \approx 0.8$ and $\nu \approx 1.2$. The decrease in ξ very near $\nu = 1$ is attributed to the decreasing density of

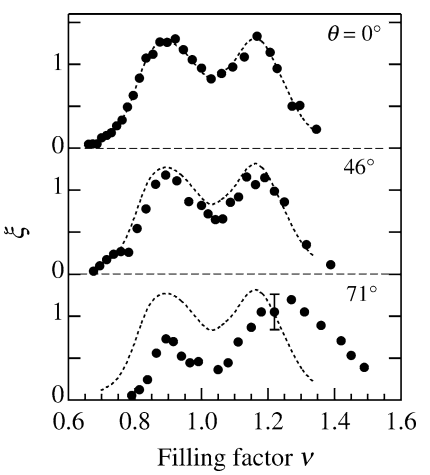

Figure 6. (a) $\xi = C/C_n^{QW}$ versus ν at $T = 60$ mK and indicated tilt angles (sample M280). The ξ-envelope for $\theta = 0°$ (dotted line), is shown for comparison.

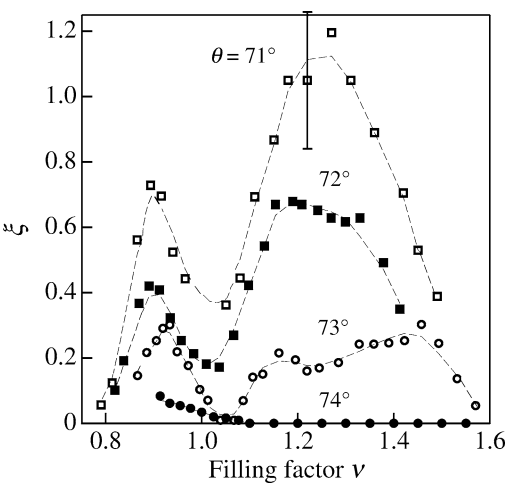

Figure 7. $\xi = C/C_n^{QW}$ versus ν at $T = 60$ mK for $71° \lesssim \theta \lesssim 74°$ (sample M280). The dashed lines are guides to the eye.

skyrmions [5]. The non-vanishing ξ at $\nu = 1$ could arise from density inhomogeneities across the measured specimens, resulting in a finite density of skyrmions at nominal filling factor $\nu = 1$. It should be mentioned that for sample M280, ξ at maxima reaches values above one (Fig. 6), implying that the measured heat capacity exceeds that of the QWs' nuclei. Besides the experimental accuracy ($\pm 10\%$) and uncertainty in well-width ($\pm 10\%$), the barriers' nuclei may enhance the measured C because of the penetration of the electron wave function into the $Al_{0.1}Ga_{0.9}As$ barriers and because of nuclear spin diffusion across the QW–barrier interface in the time scale of the experiment.

We now address the important theoretical prediction that a transition from skyrmions to single spin–flip excitations is expected above a critical $\tilde{g}$ ($\tilde{g}_c$) [4]. Here $\tilde{g} = |g^*|\mu_B B/[e^2/(\epsilon l_B)]$ is the ratio between Zeeman and Coulomb energy, $|g^*|\mu_B = 0.3$ K/T, $\epsilon \approx 13\epsilon_0$, $l_B = (\hbar/eB_\perp)^{1/2}$ is the magnetic length, and $B_\perp$ is the perpendicular component of the magnetic field. Figures 6 and 7 capture the evolution of ξ versus ν with tilt angle at $T = 60$ mK. As seen in Fig. 6, ξ versus ν at $\theta = 46°$, is nearly identical to the $\theta = 0°$ data. On the other hand, at $\theta = 71°$, the data show a significant asymmetry with respect to the $\nu = 1$ position and a broadening of the $\nu > 1$ peak. For $\nu < 1$, ξ at $\nu \approx 0.9$ is reduced by a factor of 2 when compared to the $\theta = 0°$ value and it vanishes for $\nu \lesssim 0.8$. Most remarkable, however, is that the magnitude of ξ at the $\nu > 1$ peak is comparable to the $\theta = 0°$ data, implying a still strong coupling of the nuclei to the lattice.

When θ is further increased above 71° only by few degrees, the nuclear heat capacity decreases dramatically for all investigated ν (Fig. 7). For $\theta \gtrsim 74°$, the nuclear heat capacity is no longer detectable up to the highest studied tilt angle (77°). To bring into focus the evolution of the coupling between the nuclear spin system of GaAs QWs and the lattice with θ (and $\tilde{g}$), we plot ξ at $\nu > 1$ and $\nu < 1$ maxima versus $\tilde{g}$ (Fig. 8). The coupling due to low-energy electron spin excitations is progressively suppressed for $\tilde{g} \gtrsim 0.035$ and it vanishes in the range $0.037 \lesssim \tilde{g} \lesssim 0.043$. We believe that this behavior provides evidence for the *transition from skyrmions to single spin–flip excitations* at $\tilde{g}_c \approx 0.04$ in our sample. This transition is quite abrupt: the disappearance of the nuclear spin contribution of GaAs QWs to the measured heat capacity occurs in a narrow $\tilde{g}$-range. The measured $\tilde{g}_c$ is smaller than the theoretical $\tilde{g}_c = 0.054$ calculated for the skyrmion to single spin–flip transition for an *ideal* 2DES [27]. We recount that several factors, however, are expected to reduce $\tilde{g}_c$ for a *real* 2DES, including the finite thickness of the electron layer, Landau level mixing, and disorder. Indeed, calculations by Cooper [28] reveal that taking into account the finite z-extent of the 2DES *alone* leads to $\tilde{g}_c = 0.047$, closer to our experimental value. The inclusion of the Landau level mixing will further push down $\tilde{g}_c$ to ≈ 0.042 [29]. It is worth emphasizing that calculations are usually performed at $\nu = 1$ while the heat capacity data of Figs. 6 and 7 provide values for $\tilde{g}_c$ in the full ν-range ($0.8 \lesssim \nu \lesssim 1.2$) where skyrmions (or anti-skyrmions) are expected in the ground state of the 2DES. In particular, we observe that $\tilde{g}_c$ depends on ν; it increases from $\tilde{g}_c \approx 0.037$ at $\nu = 1.2$ to $\tilde{g}_c \approx 0.043$ at

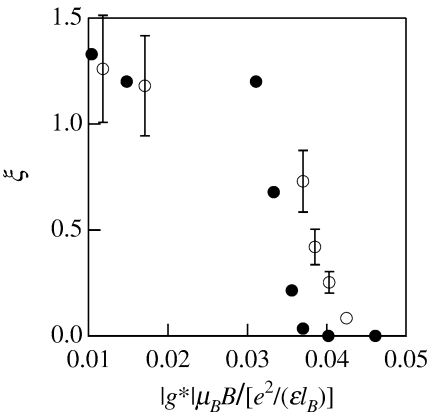

Figure 8. $\xi = C/C_n^{QW}$ at $\nu > 1$ (•) and $\nu < 1$ (○) maxima is plotted vs $\tilde{g} = |g^*|\mu_B B/[e^2/(\epsilon l_B)]$ at $\theta = 0°$, $\theta = 46°$, and $\theta \gtrsim 71°$ (sample M280).

$\nu = 0.9$. The different $\tilde{g}_c$ observed at $\nu < 1$ and $\nu > 1$ could be brought into connection with the absence of the particle–hole symmetry around $\nu = 1$, favored by the tilted magnetic fields.

4.2. Nuclear spins and the fractional QHE state at $\nu = 4/3$

The reentrant behavior of the $\nu = 4/3$ state is displayed in Figs. 2 and 9(a). Destruction of the $4/3$ structure for $\theta \gtrsim 65°$ is consistent with a spin-unpolarized ground state at small θ as increasing the Zeeman energy forces the system into a different spin state (presumably, partially polarized). The $4/3$ state collapses from $\Delta_{4/3} = 440$ mK to zero over the magnetic field range 2.8–6.5 T, it is absent for $6.5 \lesssim B \lesssim 8.8$ T, and re-emerges for $B \gtrsim 8.8$ T. Our observations are too scant to speculate on the detailed nature of the reentrant $4/3$ state.

Examining the heat capacity data of Figs. 6 and 7 we observe a broadening of the $\nu > 1$ C-peak, starting with $\theta \approx 61°$. Figure 8 shows the reduction of the $\nu > 1$ C-peak for $\theta \gtrsim 72°$. Therefore, these data seem to support the idea that a nuclear heat capacity is observed near $\nu = 4/3$ for a finite range of tilt angles. Why? A possible escape from this enigma is provided by the tilted magnetic field transport data, exhibiting a re-entrant behavior of the $\nu = 4/3$ fractional QHE state. The evolution of ξ with B near $\nu = 4/3$ is presented in Fig. 9(b). Our tilted-magnetic field heat capacity data near $\nu = 4/3$ uncover a rapid nuclear spin–lattice relaxation for all nuclei in the QWs in the B-range where the $\nu = 4/3$ fractional QHE state is absent. This behavior signals the presence of nearly gapless spin fluctuations in the 2DES when the $\nu = 4/3$ fractional QHE state undergoes a spin phase transition from a spin-unpolarized ground state to a partially polarized ground state. The existence of low-energy spin fluctuations (which are no longer constraint by a finite excitation gap) permit then the strong coupling of the 2DES to the GaAs QWs' nuclei. We note that for particular values of $\tilde{g}$ and in the presence of many skyrmions at $\nu > 1$ one may also expect that various skyrmion lattices form in the limit of zero temperature. Some of these lattices support *two* Goldstone modes associated with the broken spin rotational and translational symmetry [5]. Therefore, the fact that C peaks near $\nu = 4/3$ could also mean that the multi-skyrmion phase at $\nu > 1$ allows a stronger coupling to the nuclei in the range of magnetic fields from 6.5 to 8.8 T.

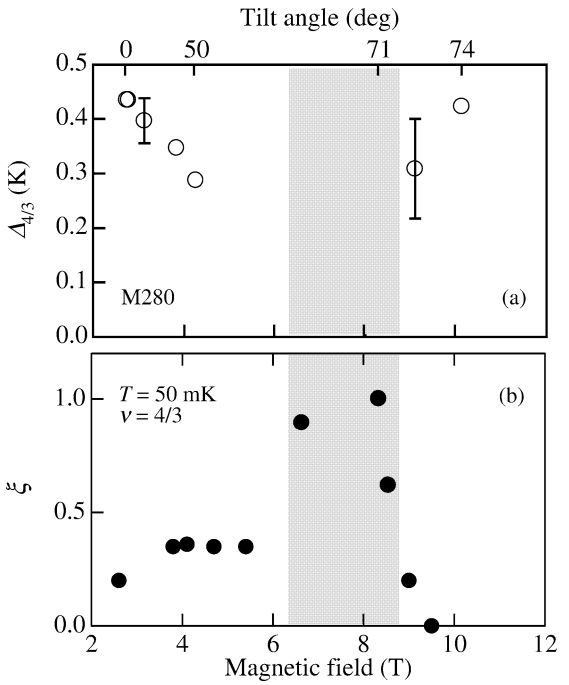

Figure 9. Panel (a) shows the B-dependence of $\Delta_{4/3}$. Panel (b) displays the B-dependence of ξ near $\nu = 4/3$, measured at $T = 50$ mK. The grey regions in panels (a) and (b) indicate the B-range where the $\nu = 4/3$ fractional QHE state is absent (sample M280).

5. Conclusions

In conclusion, our heat capacity data underscore the importance of the coupling between the 2DES and nuclear spins, and point to the rich physics of the ground and excited states of the 2DES near $\nu = 1$. For $\nu \approx 0.8$ and $\nu \approx 1.2$, C exhibits a striking T-dependence, including a remarkably sharp peak at very low temperature suggestive of a *phase transition in the 2DES*. We interpret these unexpected observations in terms of the Schottky model for the nuclear-spin heat capacity of Ga and As atoms which couple to the lattice via the 2DESs' low-energy spin-texture excitations (skyrmions). Our experiments show that the sharp peak in C versus T near $\nu = 1$ is due to the nuclei in the thick barriers between the GaAs quantum wells. Heat capacity measurements also reveal the absence of the nuclear spin contribution of GaAs QWs to the measured heat capacity as $\tilde{g}$ exceeds a critical value $\tilde{g}_c \approx 0.04$. This absence suggests the suppression of the skyrmion-mediated coupling between the lattice and the nuclear spins as the spin excitations of the 2DES make a transition from skyrmions to single spin–flips above $\tilde{g}_c$. The role of nuclear spin degree freedom for the physics of the $\nu = 4/3$ QHE state has been illustrated. Searching for T- and θ-dependent hysteretic behavior near $\nu = 4/3$ in samples M242 and M280 may shed further light on the participation of the nuclear spins in spin phase transitions of unpolarized fractional QHE states.

Acknowledgements. The authors are grateful to S.M. Girvin, A.H. MacDonald, and N.R. Cooper for valuable discussions. S.M. and V.B. are much indebted to E. Grivei and J.-M. Beuken for help with experiments. The work performed in Louvain-la-Neuve was supported by 'Action de Recherche Concertée' and the programme 'PAI' sponsored by the 'Communauté Française de Belgique'.

References

[1] K. von Klitzing, G. Dorda, M. Pepper, Phys. Rev. Lett. 45 (1980) 494.
[2] D.C. Tsui, H.L. Stormer, A.C. Gossard, Phys. Rev. Lett. 48 (1982) 1559.
[3] B.I. Halperin, Helv. Phys. Acta 56 (1983) 75.
[4] S.L. Sondhi, A. Karlhede, S.A. Kivelson, E.H. Rezayi, Phys. Rev. B 47 (1993) 16419.
[5] S.M. Girvin, in: A. Comtet, T. Jolicoeur, S. Ouvry, F. David (Eds.), Topological Aspects of Low Dimensional Systems, Proceedings of the Les Houches Summer School of Theoretical Physics, Session LXIX, 1998, Springer-Verlag and EDP Sciences, 1999, p. 53.
[6] A. Schmeller, J.P. Eisenstein, L.N. Pfeiffer, K.W. West, Phys. Rev. Lett. 75 (1995) 4290.
[7] S.E. Barrett, G. Dabbagh, L.N. Pfeiffer, K.W. West, R. Tycko, Phys. Rev. Lett. 74 (1995) 5112.
[8] R. Tycko et al., Science 268 (1995) 1460.
[9] P. Khandelwal, A.E. Dementyev, N.N. Kuzma, S.E. Barrett, L.N. Pfeiffer, K.W. West, Phys. Rev. Lett. 86 (2001) 5353.
[10] V. Bayot, E. Grivei, S. Melinte, M.B. Santos, M. Shayegan, Phys. Rev. Lett. 76 (1996) 4584.
[11] V. Bayot, E. Grivei, J.-M. Beuken, S. Melinte, M. Shayegan, Phys. Rev. Lett. 79 (1997) 1718.
[12] S. Melinte, E. Grivei, V. Bayot, M. Shayegan, Phys. Rev. Lett. 82 (1999) 2764.
[13] E.H. Aifer, B.B. Goldberg, D.A. Broido, Phys. Rev. Lett. 76 (1996) 680.
[14] I.V. Kukushkin, K. von Klitzing, K. Eberl, Phys. Rev. B 60 (1999) 2554.
[15] S. Melinte, N. Freytag, M. Horvatić, C. Berthier, L.P. Lévy, V. Bayot, M. Shayegan, Phys. Rev. B 64 (2001) 085327.
[16] J.P. Eisenstein, H.L. Stormer, L.N. Pfeiffer, K.W. West, Phys. Rev. B 41 (1990) 7910.
[17] L.W. Engel, S.W. Hwang, T. Sajoto, D.C. Tsui, M. Shayegan, Phys. Rev. B 45 (1992) 3418.
[18] S. Kronmüller, W. Dietsche, J. Weis, K. von Klitzing, W. Wegscheider, M. Bichler, Phys. Rev. Lett. 81 (1998) 2526.
[19] S. Kronmüller, W. Dietsche, K. von Klitzing, G. Denninger, W. Wegscheider, M. Bichler, Phys. Rev. Lett. 82 (1999) 4070.
[20] J.H. Smet et al., Nature 415 (2002) 218.
[21] A. Abragam, Principles of Nuclear Magnetism, Oxford Univ. Press, New York, 1961.
[22] R.G. Clark, S.R. Haynes, A.M. Suckling, J.R. Mallett, P.A. Wright, J.J. Harris, C.T. Foxon, Phys. Rev. Lett. 62 (1989) 1536.
[23] R.R. Du, A.S. Yeh, H.L. Stormer, D.C. Tsui, L.N. Pfeiffer, K.W. West, Phys. Rev. Lett. 75 (1995) 3926.
[24] M. Shayegan, J.K. Wang, M. Santos, T. Sajoto, B.B. Goldberg, Appl. Phys. Lett. 54 (1989) 27.
[25] A.M. Lanzillotto, M. Santos, M. Shayegan, J. Vac. Sci. Technol. A 8 (1990) 2009.

[26] G.S. Boebinger et al., Phys. Rev. B 36 (1987) 15.
[27] N.R. Cooper, Phys. Rev. B 55 (1997) R1934.
[28] N.R. Cooper, Private communication.
[29] V. Melik-Alaverdian, N.E. Bonesteel, G. Ortiz, Phys. Rev. B 60 (1999) R8501.